This article has been accepted for publication in IEEE Transactions on Industrial Electronics. This is the author's version which has not been fully edited and content may change prior to final publication. Citation information: DOI 10.1109/TIE.2021.3097610

Modular Power Sharing Control for Bearingless Multi-Three Phase Permanent Magnet Synchronous Machine

Zhuang Wen, *Student Member, IEEE*, Mauro Di Nardo, *Member, IEEE*, Giacomo Sala, *Member, IEEE*, Giorgio Valente, Alessandro Marfoli, Michele Degano, *Member, IEEE*, Pericle Zanchetta, *Fellow, IEEE*, Chris Gerada, *Senior Member, IEEE*.

***Abstract*—This paper proposes a modular approach to the power sharing control of permanent magnet synchronous bearingless machine. The selected machine topology features a winding layout with phases distributed into non-overlapping three phase groups, a solution whose twofold aim is to increase the fault tolerance and to allow for the radial force generation. The three phase sub-windings are supplied by standard three-phase inverter, leading to a modular system architecture.**

A throughout explanation of the methodology used to develop the control algorithm is presented considering the torque and force control in combination with the power sharing management of the machine. Special emphasis is also placed on validating the modelling hypotheses based on a finite element characterisation of the machine electro-mechanical behaviour. The proposed control strategy is also extended to cater the possibility of one or more inverters failure, thus validating the intrinsic advantage of the redundancy obtained by the modularity of the system.

An extensive experimental test campaign is finally carried out on a prototyped multi-three phase permanent magnet synchronous drive. The obtained results validate the bearingless power sharing operation in healthy and faulty scenarios, both at steady state and under extreme transient condition.

***Index Terms*—Bearingless motor, magnetic suspension, multi phase drives, finite element analysis, power sharing, fault tolerant control.**

I. Introduction

MULTI-PHASE electric drives are recognised for featuring enhanced performance and fault tolerant capability when compared with conventional three phase counterparts [1]. They have been historically adopted in high power applications, such as large generators, ships and trains propulsion [2] mainly thanks to the possibility of splitting the power (both current and/or voltage) among multiple phases which allows overcoming power electronics' limitations [3]. Lately, this machine topology has also been adopted in automotive powertrains [4].

A myriad of winding layouts are possible with multiple phases with both overlapped and non-overlapped arrangements differing by the number of phases and their spatial distribution [5]. The layouts can all be conceptually classified according to the electrical angle between the magnetic axes of consequent phases. This angle is often $360/n$ or $180/n$, being n the total number of phases. However, it can vary according to the number of stator slots and rotor poles. A further multi-phase winding variant, usually called with different names (asymmetrical, split-phase, multi-m phase, etc.), is obtained by subdividing the n phases into N sets of m phases. This represents an interesting solution widely adopted in commercial products. In fact, when $m = 3$ conventional three phase converters can be employed to supply the multi-three phase windings [6]. An interesting feature of multi m-phase machines is the possibility of independently managing the power flows among the different three-phase sub-windings, hence achieving the so called power sharing operation [7], [8]. The latter provides the possibility that m-phase sub-windings can be simultaneously supplied by diverse inverters, due to a drive architecture layout that, for example, can present more independent power sources. Particularly, the power sharing technique is important in applications requiring a high level of reliability [9]. An attempt to further increase the fault tolerant feature of this winding topology is to physically distribute the m-phase sub-windings into N non-overlapped sets [10], resulting in physical and thermal insulation [11], [12]. Along with the higher fault tolerance, this modular multi-phase winding layout presents the further advantage of being able to generate controllable radial forces beside the torque [13], [14]. This additional feature makes this winding layout suitable for bearingless or bearing relief operation in application requiring a high level of reliability [15].

Bearingless operation is particularly convenient in high speed applications [16] or in aseptic environments [17]. Two three-phase windings featuring different number of poles were initially employed to generate independent torque and suspension force [18] leading to a reduced stator slot utilisation hence decreasing the machine power density. More recently, mainly three combined winding solutions have been proposed, where each winding set contributes to both torque and suspension force production, namely the bridge-configured winding [19],

Zhuang Wen, Mauro Di Nardo, Alessandro Marfoli, Michele Degano and Chris Gerada are with Department of Electrical and Electronic Engineering, University of Nottingham, UK. (email: zhuang.wen@nottingham.ac.uk; mauro.dinardo4@nottingham.ac.uk; alessandro.marfoli1@nottingham.ac.uk; michele.degano@nottingham.ac.uk; chris.gerada@nottingham.ac.uk)

Giacomo Sala is with the Department of Electrical, Electronic, and Information Engineering "Guglielmo Marconi" - DEI, University of Bologna, Italy. (email: g.sala@unibo.it)

Giorgio Valente is with Romax Technologies, Nottingham, NG7 2TU, UK. (email: giorgio.valente@romaxtech.com)

Pericle Zanchetta is with Department of Electrical and Electronic Engineering, University of Nottingham, UK and Department of Electrical, Computer and Biomedical Engineering, University of Pavia, Italy (email: pericle.zanchetta@nottingham.ac.uk)

the parallel-configured winding [20] and the multi-phase winding [21]. A comprehensive comparison is presented in [22] showing that there is no clear winner, i.e. a configuration requiring the least components number, the easiest control implementation and the highest fault tolerance. This conclusion makes the modular multi-m phase winding a serious contender in fault tolerant bearingless applications.

This particular drive architecture has already been investigated in [23] for a bearingless application with power sharing capability among modules. However, the presented control strategy was based on the vector space decomposition approach. The latter treats the whole winding layout as a unique system thus loosing the modular approach making the fault tolerant control more complex and challenging.

This paper presents a modular power sharing control strategy of a multi-three phase surface mounted permanent magnet synchronous (SMPM) machines suitable for bearingless operation. The proposed control is fully based on the modularity of the multi three-phase drive extending the conventional bearingless control to the management of power sharing among the subwinding and to the fault tolerant control acting in case of module open-phase fault. First, a detailed modelling of the machine electro-mechanical behaviour is described in Section II aided by a finite element analysis (FEA) of the considered machine. Section III outlines the implemented control strategies allowing the power sharing among stator modules during bearingless operation in both healthy and faulty conditions. Then, a brief overview of the control architecture is presented in Section IV along with a detailed finite element analysis (FEA) aimed at assessing the effects of neglecting the mutual interaction among stator modules and the effect of increasing the harmonic content included in the control. Finally, Section V reports an extensive test campaign on a prototyped machine validating the bearingless power sharing operation in healthy and faulty scenarios, both at steady state and transient conditions.

II. Modular Approach to the Production of Radial Force and Torque in Multi-Three Phase SMPM

A. Machine Structure

The modular bearingless SMPM machine is illustrated in Fig. 1 a). The machine is divided into three equal portions occupied by three three-phase windings and highlighted in red, blue and yellow, respectively. Each three-phase winding is star-connected with a galvanically isolated neutral point. The symbol $+$ and $-$ indicate the directions of the currents, flowing out and into the plane of the paper, respectively, while the subscript $i \in [1\,,2\,,3]$ is adopted to define the numerical order of the winding module. For example, $+u_1$ means the current direction of the first module phase u is flowing out the plane of the paper. Finally, the main parameters of the machine are listed in Table I.

TABLE I
Machine Parameters

Parameter	Value
Pole number ($2p$)	6
Power rating	1.5 kW
Rated speed (n_{rated})	3000 r/min
Rated torque	5 Nm
Rated machine current	13 A
Torque constant (k_T)	0.128 Nm/A
Line to line voltage constant (k_V)	15.5 V/krpm

B. Mathematical model

The definition of the machine model is the first step required to analyse the electromagnetic behaviour of an electric motor, whose understanding is essential for the development of a suitable control algorithm. Owing to the modularity of the multi three-phase SMPM machine, the model can be easily defined as function of the $d-q$ axis variables of each three-phase subwinding (with the d-axis aligned with the centre of the north pole of the rotor magnets).

The key inputs of the multi three-phase SMPM machine model are the d-q axis currents of each module, whereas the outputs are the mechanical forces and torque acting on the rotor, hereinafter referred as wrench W. The latter can be defined as a vector of the $x-y$ components of the radial force (F_x, F_y) and the torque T acting on the rotor:

$$W = [F_x, F_y, T]' \tag{1}$$

where $'$ is the transpose operator. The relationships between the $d-q$ currents of the general $i-th$ sector $({}^i i_d, {}^i i_q)$ and the respective contribution to the wrench of the multi three-phase SMPM motor is function of both axis currents and rotor electrical position, as follows:

$${}^i W = [{}^i F_x, {}^i F_y, {}^i T]' = f({}^i i_d, {}^i i_q, \vartheta_e) \tag{2}$$

Under linear operating conditions and neglecting the force contributions due to the interactions between stator m.m.f. harmonics, the wrench produced by the entire machine can be considered the sum of the effects of all the N sub-modules supplied with the respective $d-q$ currents:

$$W = \sum_{i=1}^{N} {}^i W = \sum_{i=1}^{N} {}^i f({}^i i_d, {}^i i_q, \vartheta_e) \tag{3}$$

The functions ${}^i f$ can be evaluated by accurate analytical models or, for a better accuracy, through FE simulations. Although analytical approaches are computationally efficient, their results needs to be FE validated [24]. For this reason, in

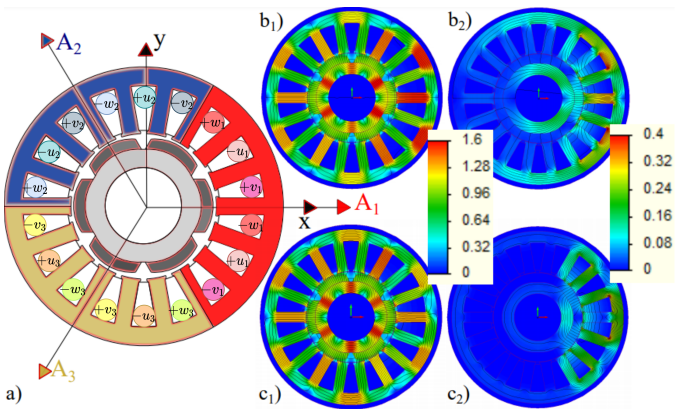

Fig. 1. a) Cross-section of the multi three-phase SMPM machine, b_1) and c_1) flux density distributions when the first module is supplied with the rated d and q currents, b_2) and c_2) flux density maps without PM contribution.

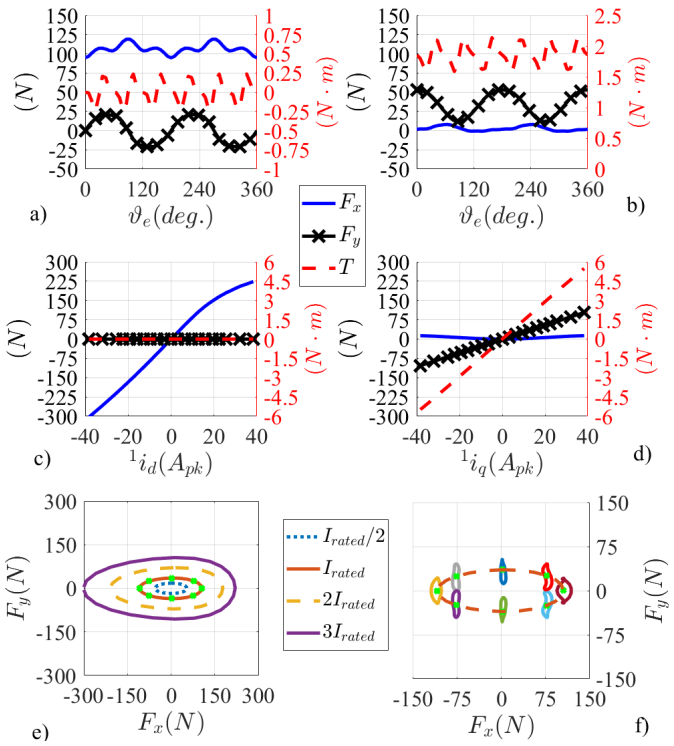

Fig. 2. Identification of the wrench produced by the first module: a,b) as function of the rotor position when supplied with the rated d and q currents, respectively; c,d) and as function of the d and q axes currents averaging the rotor position dependency; e) average force locus in the force plane as the current phase angle increases for different given current modules; f) force locus as function of the rotor position for different current phase angles.

the following, the characterisation of the considered machine, whose details are reported in Table I, is carried out via 2D FEAs (with the commercial suite MagNet©). Fig. 2 reports the wrench components of the first module of the machine considered throughout this study (whose first phase is placed on the x-axis as shown in Fig. 1a). In particular, Fig. 2a) and b) show the wrench components as function of the rotor electrical position when supplied by rated d and q axis current, respectively. Both force components feature a relevant second harmonic whereas the torque, as expected, is dominated by the sixth harmonic. Fig. 1b_1) and c_1) report the flux density distributions when supplying positive d and q axis rated current, respectively, while sub-figures b_2) and c_2) show the same distributions without the permanent magnet contributions. From these flux maps it is also possible to appreciate that the soft magnetic material is mainly operating in its linear range. Fig. 2c) and d) depict the average wrench components as function of the both d and q axis currents, respectively. It can be noticed that torque and force contributions vary almost linearly with the currents up to double the rated value (i.e. $26A_{pk}$). Above this value, the saturation of the flux path has a relevant effect only when supplying with positive $d-$axis current (i.e. when strengthening the PM flux). Consequentially, neglecting the reluctance torque, the wrench contribution of each module can be assumed linearly dependent on the respective currents, and so the following matrix equation can be written:

$$^1W(^1i_d, ^1i_q, \vartheta_e) = {}^1K_{dq}(\vartheta_e)\begin{bmatrix}^1i_d & ^1i_q\end{bmatrix}' \tag{4}$$

where $^1K_{dq}(\vartheta_e)$ is a 3×2 matrix of wrench coefficients only function of the rotor electrical position (ϑ_e). This approximation is strictly valid when working within the liner region of the wrench-current relationship reported in Fig. 2c) and d). Outside this area, each coefficient of the matrix $^1K_{dq}$ would mainly depend from the respective current (e.g. $^1k_{Fx,d}(^1i_d)$, $^1k_{Fx,q}(^1i_q)$, etc), as shown in Fig. 2e). The latter reports the average force produced by the first stator module for a given current amplitude and different phase angles. The locus described by the force vector clearly resembles an ellipse which uniformly changes dimensions (both axes) when operating in the linear region. This implies that the force vector can be described as function of the current components via constant coefficients and so eq.(4) is valid. Outside the linear region, the force locus deviates from being an ellipse due to the unequal effect of the non linearities on the force components. Fig. 2f) shows the locus described by the force vector as function of the rotor position for the rated current condition and different current phase angles. The figure highlights the fact that the force ripple is mainly produced perpendicular to the magnetic axis of the supplied module (i.e., the y-axis for the first module).

In principle, the same identification procedure should be carried out for all the other modules of the machine. However, being each subwinding rotated with respect to the adjacent one, the wrench of the generic $i-th$ module can be evaluated by simply taking into account the mechanical shift $^i\Delta\vartheta_m$ of the considered stator module, as follows:

$$^iW(^ii_d, ^ii_q, \vartheta_e) = {}^iR\,{}^1K_{dq}(\vartheta_e)\begin{bmatrix}^ii_d & ^ii_q\end{bmatrix}' \tag{5}$$

where ^iR is a rotational matrix defined as:

$$^iR = \begin{bmatrix}\cos(^i\Delta\vartheta_m) & -\sin(^i\Delta\vartheta_m) & 0\\ \sin(^i\Delta\vartheta_m) & \cos(^i\Delta\vartheta_m) & 0\\ 0 & 0 & 1\end{bmatrix} \tag{6}$$

As an example, for the multi-sectored machine layout depicted in Fig. 1a): $^1\Delta\vartheta_m = 0$, $^2\Delta\vartheta_m = \frac{2\pi}{3}$, $^3\Delta\vartheta_m = \frac{4\pi}{3}$.

The overall wrench produced by all the modules results from (3) and (5) as follows:

$$W = \sum_{i=1}^{N} {}^iK_{dq}(\vartheta_e)\begin{bmatrix}^ii_d & ^ii_q\end{bmatrix}' = K_{dq}(\vartheta_e)i_{dq} \tag{7}$$

where the K_{dq} is a $3 \times 2N$ matrix built by pending the columns of the $^iK_{dq}(\vartheta_e)$ matrices obtained by (5), while the total current vector is $i_{dq} = [^1i_d, ^1i_q, ^2i_d, ^2i_q, ..., ^Ni_d, ^Ni_q]'$. The assumption underling eq.(3), i.e., neglecting the mutual interactions among the machine submodules, will be further analysed and validated in section IV.

III. Control Strategies

Once the wrench-current function is identified, its inversion needs to be carried out in order to control the machine, i.e. find the current set points which generate a given reference wrench (W^*). Being the wrench-current relationship (7) an underdetermined system, its inverse problem has more than one solution, i.e. there exist ∞^{2N-3} current solutions providing the same wrench ($2N-3$ is the number of unknown minus the number of equations). Among all the possible solutions

This article has been accepted for publication in IEEE Transactions on Industrial Electronics. This is the author's version which has not been fully edited and content may change prior to final publication. Citation information: DOI 10.1109/TIE.2021.3097610

to this kind of control problems, the result that minimises the stator copper loss is recognised as valuable one within the field of multi-phase machines control [8]. This approach allows fully exploiting the various sub-windings capability with a closed form relationship between currents and wrench. In fact, supposing that the solution to the underdetermined system (7) has also to satisfy the objective of minimising the joule losses ($P_{J,tot}$), the problem to solve can be expressed as:

$$\begin{aligned} &min\ P_{J,tot} = {i'}_{dq} \cdot R_S \cdot i_{dq} \\ &s.t.\ W^* = K_{dq}(\vartheta_e) \cdot i_{dq} \end{aligned} \tag{8}$$

where R_S is the diagonal matrix of the phase resistances. The latter (8) is a classic quadratic optimisation problem which can be solved applying the Langrange multiplier method, leading to the well-known result:

$$i^*_{dq} = K'_{dq}(\vartheta_e)[K_{dq}(\vartheta_e)K'_{dq}(\vartheta_e)]^{-1}W^* = K^+_{dq}(\vartheta_e)W^* \tag{9}$$

where K^+_{dq} is the Moore-Penrose inverse of the matrix K_{dq}. In general, the Moore-Penrose inverse represents the solution of an undetermined system of equation minimising the square of the input variables, which in this case is proportional to the stator Joule loss $P_{J,tot}$.

As previously mentioned, this is not the only way to solve this class of problems. Although it allows a computational efficient implementation leading to the maximisation of the operational efficiency, it does not directly consent to control the power flows among the several sub-modules as desired in application requiring power sharing operation. In the following two subsections, this control strategy is extended in order to consider the power sharing constraints and the open fault of an entire stator module.

A. Power sharing operation

The power sharing operation can be defined by introducing the vector of the sharing coefficients $Z_{sh} = [{}^1z_{sh}, {}^2z_{sh}, ..., {}^Nz_{sh}]'$ determining the reference q axis currents $i^*_q = [{}^1i^*_q, {}^2i^*_q, ..., {}^Ni^*_q]'$ as follows:

$$\begin{aligned} &i^*_q = \tfrac{T^*}{K_T} Z_{sh} \\ &s.t. \textstyle\sum_{i=1}^{N} {}^iz_{sh} = 1 \end{aligned} \tag{10}$$

where K_T is the torque constant and T^* is the reference torque. The imposition of the q axis currents via the sharing coefficients fully determine the torque produced by the machine. However, these current components also create a radial force contribution (F_q) which can be evaluated via the eq. (7). More precisely, only the even columns of the K_{dq} matrix and the first two rows are needed to evaluate this force contribution. By building up this new sub-matrix $K_q(\vartheta_e)$, the force contributions F_q are expressed as follows:

$$F_q(\vartheta_e) = \begin{bmatrix} F_{x,q} & F_{y,q} \end{bmatrix}' = K_q(\vartheta_e) i_q \tag{11}$$

The remaining degrees of freedom of the system, i.e. the d-axis currents, can be exploited for the production of the reference radial forces (F^*). Indeed, the d axis currents i_d produce radial force components which can be evaluated from (7):

$$F_d(\vartheta_e) = \begin{bmatrix} F_{x,d} & F_{y,d} \end{bmatrix}' = K_d(\vartheta_e) i_d \tag{12}$$

where K_d is the sub-matrix of K_{dq} built with its odd columns and the first two rows. In order to produce the desired force reference F^* equal to the sum of the d and q axis currents contributions (F_d and F_q), the reference d axis currents have to produce the force $F^* - F_q$, therefore:

$$i^*_d(\vartheta_e) = K^+_d(\vartheta_e)[F^* - F_q(\vartheta_e)] \tag{13}$$

where $K^+_d(\vartheta_e)$ is the Moore-Penrose inverse of the $3 \times N$ $K_d(\vartheta_e)$ matrix. It is worth to underline that the d-axis currents do not have any effect on the torque, being the reluctance torque null. Fig. 3 summarises the proposed bearingless power sharing control strategy for the triple three-phase permanent magnet machine considered in this study.

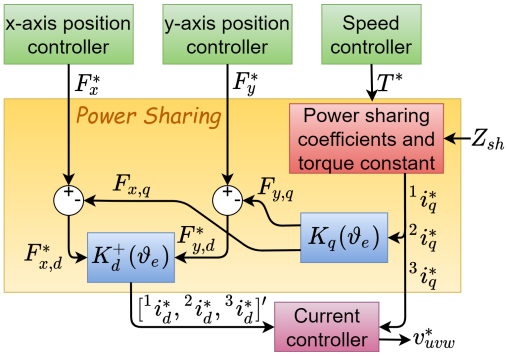

Fig. 3. Flow chart of the power sharing technique.

B. Module open fault condition

Due to the modularity of the torque and force generation of this particular machine topology, it is possible to keep on fully controlling force and torque in power sharing operation also when an entire sub-winding is opened. In fact, the control problem outlined in the previous subsection can be easily solved by assuming a reduced number of three-phase subsystems. Indeed, while building the matrix of wrench coefficients K_{dq}, the sub-matrix ${}^iK_{dq}$ of the faulty module must not be considered.

In case of open fault of the first module (but the same procedure can be extended to the other ones), the considered machine would feature two sharing coefficients ${}^2z_{sh}$ and ${}^3z_{sh}$, with ${}^3z_{sh} + {}^3z_{sh} = 1$ which determine the split of the torque among the modules 2 and 3 (i.e., ${}^2i^*_q$ and ${}^3i^*_q$) while the d axis reference currents needed to produce the reference force would be:

$$i^*_d = \begin{bmatrix} {}^2i^*_d \\ {}^3i^*_d \end{bmatrix} = \begin{bmatrix} {}^2k_{1,1} & {}^3k_{1,1} \\ {}^2k_{2,1} & {}^3k_{2,1} \end{bmatrix}^{-1} \begin{bmatrix} F^*_{x,d} \\ F^*_{y,d} \end{bmatrix} \tag{14}$$

with:

$$\begin{bmatrix} F^*_{x,d} \\ F^*_{y,d} \end{bmatrix} = \begin{bmatrix} F^*_x \\ F^*_y \end{bmatrix} - \begin{bmatrix} {}^2k_{1,2} & {}^3k_{1,2} \\ {}^2k_{2,2} & {}^3k_{2,2} \end{bmatrix} \begin{bmatrix} {}^2i^*_q \\ {}^3i^*_q \end{bmatrix} \tag{15}$$

where all the wrench coefficients are still function of the rotor electrical position ϑ_e. It is worth noticing that for this particular case (i.e. 3 modules) the pseudo-inverse of the matrix is not required because the system of equations is no more underdetermined. This control approach can be used to manage open faults of more than one module, aware that to continue the bearingless operation under power sharing control the minimum number of healthy modules must be two.

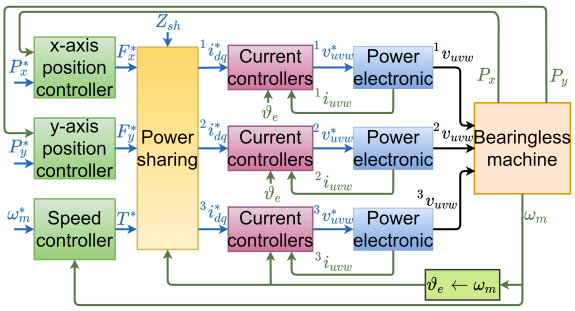

Fig. 4. Schematic diagram of the bearingless machine control system.

IV. Control Architecture and Implementation

At first, this section gives an overview of the control system architecture of the bearingless multi-three phase permanent magnet synchronous machine. Afterwards, a detailed FE based analysis is presented in order to:

- validate the assumption underling eq. (3) which neglects the interaction among the several machine sub-modules;
- determine how to implement the machine model inversion (i.e. eq. (9) or (11) and (13) if the power sharing among the modules has to be controlled) on a real time control platform.

A. Control architecture

A schematic of the bearingless control system with the power sharing among the sub-modules is illustrated in Fig. 4. The machine three phase sub-windings are supplied by three independent three phase inverters. The position controllers, i.e. two independent PID regulators and the speed loop PI controller determine the reference wrench components from the measured radial shaft positions and angular speed errors. The reference currents are then calculated via the power sharing logic detailed in Section III. The latter are then tracked via six conventional PI regulators. The gate signals of the inverter switches are then obtained through PWM from the references voltages. The current PI controllers, the position PID controllers, and the speed PI regulators are designed according to the pole placement approach.

B. Effect of increasing the detail of wrench harmonic content

The bearingless control of a multi three permanent magnet synchronous machine requires the implementation of the control strategy summarised in eq. (9) or in eq. (13) when including the power sharing option on a real time control platform. In particular, the wrench coefficients matrices K_{dq}^{+}, K_q and K_d^{+} can be calculated off-line once the full matrix K_{dq} has been characterised by FEA or experimental tests. Such matrices, function of the rotor position, can be then stored via Look Up Tables (LUT) on the real time hardware in order to perform the bearingless power sharing control. However, this approach would lead to a significant computational burden given the dimension of these LUTs. In the attempt of relieving this implementation cost, the effect of considering a reduced harmonic content for each element of the wrench coefficient matrix K_{dq} is hereafter reported. In fact, the generic element $k_{r,c}$ of the matrix K_{dq} placed in the row r and column c can be expressed as function of the rotor electrical position ($\vartheta_e = p\vartheta_m$):

$$k_{r,c}(\vartheta_e) = \sum_{\rho=0}^{\infty} k_{r,c}(\rho) \cdot cos(\rho\vartheta_e + \varphi_{r,c}(\rho)) \qquad (16)$$

Indeed, considering only the DC component of each coefficient would lead to a massive size reduction of the LUT because K_{dq} would not depend anymore from the rotor electrical position. However, this implies disregarding all the ripple force and torque shown in Fig. 2a) and b). In this simplified case, the reference d and q axis currents providing a given wrench W^* (e.g. $F_x^* = 0N$, $F_y^* = 20N$, $T^* = 5Nm$) are independent from the rotor electrical position as shown in Fig. 5a), but the consequent produced wrench feature a significant ripple, as depicted in Fig. 5b). The latter also reports the FE-calculated (marked lines) wrench components which match quite well the expected values. The small differences between the expected and the FE values are due to the assumption on which the modelling is based, i.e. null mutual effect among modules.
When considering all the harmonic content of the wrench coefficients $k_{r,c}$, the force ripple drastically decreases as visible in Fig. 5f). However, this comes at the cost of a higher computational burden being K_{dq} dependant from the rotor position. In addition, including all the harmonics leads to more frequency components in the reference currents, as shown in Fig. 5e), which could be difficult to track at high rotational speed. It is worth to underline that the small deviations between the expected and FE calculated wrench components still remains also when considering the full harmonic spectrum of all $k_{r,c}$. From the previous analyses, these differences are mainly attributed to the mutual interaction among the stator modules. In addition, the torque ripple is almost not affected by the introduction of more harmonics due to the fact that it is mainly due to the cogging effect (no load torque).
A compromise solution between quality of the produced wrench and computational burden consists in considering only the DC and the second (with reference to the electric period) harmonic of each $k_{r,c}$ coefficient, as shown in Fig. 5c) and d). The only detrimental effect of this approximation is a slight increase of the force ripple compared with the ideal control solution. As a result, each element of the Moore-Penrose matrices K_{dq}^{+} and K_d^{+} can be expressed as function of the rotor position in electrical degrees as follows:

$$k_{r,c}^{+}(\vartheta_e) = k_{r,c}^{+}(0) + k_{r,c}^{+}(2) \cdot cos(2\vartheta_e + \varphi_{r,c}(2)) \qquad (17)$$

which can be implemented only storing the values $k_{r,c}^{+}(0)$ and $k_{r,c}^{+}(2)$ for each of the 18 wrench coefficients $k_{r,c}^{+}$.
Fig. 5a-f) refer to the standard bearingless control of a multi-three phase permanent magnet synchronous machine without the possibility to manage the power flows among stator modules. Fig. 5g,h) report the reference currents and the expected and FE wrench components when considering a non uniform power sharing scenario ($Z_{sh} = [0.4\ 0.35\ 0.25]'$). Although the references are calculated considering only the main two harmonics in each wrench coefficient $k_{r,c}$, the d axis currents include more than two harmonics. This is because the Moore-Penrose inverse of the K_d matrix (having each element sum of

This article has been accepted for publication in IEEE Transactions on Industrial Electronics. This is the author's version which has not been fully edited and content may change prior to final publication. Citation information: DOI 10.1109/TIE.2021.3097610

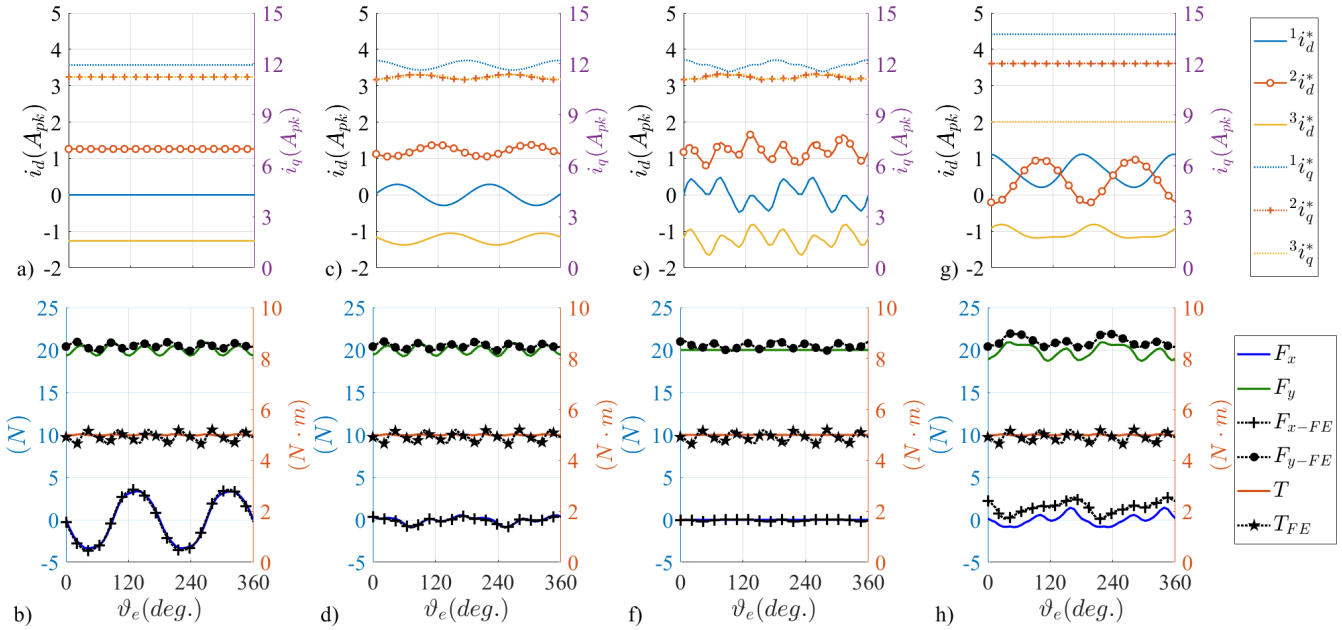

Fig. 5. Reference $d-q$ currents, expected and FE wrench components when generating the rated wrench ($F_x^* = 0N$, $F_y^* = 20N$, $T^* = 5Nm$) considering the DC components of the wrench coefficients (a,b), only the DC and 2^{nd} harmonics (c,d) and all harmonics (e,f), with power sharing (g,h).

2 harmonics) leads to matrix coefficients featuring a different harmonic content. In other words, the Moore-Penrose matrix operator does not guarantee the preservation of the harmonic spectrum of the coefficients of the inverted matrix.
Also, the differences between the expected and FE wrench components show a higher error when a non uniform power sharing scenario is considered.
It is worth to underline that the wrench mismatch between expected and FE/real values, due to the assumption of negligible interaction among stator modules, is compensated by the actions of the position and speed closed-loop controllers. Consequentially, the experimental d and q axis currents reference are expected to feature a higher harmonic content with respect to the predicted ones, shown in Fig. 5c) and g).

V. Experimental Validation

The proposed power-sharing technique is validated on a 1.5kW-3000rpm prototype bearingless multi-three phase permanent magnet synchronous machine whose parameters are listed in Table I. In the next subsections, first a general description of the experimental setup is given and then an extensive test campaign is reported to fully validate the proposed control strategy. In particular, three tests are implemented to verify the performance of the proposed bearingless power sharing control technique in different healthy and faulty operating scenarios.

A. Instrumented test rig

The stator of the proposed bearingless SMPM machine is displayed in Fig. 6. It is clearly observed that three three-phase windings are galvanically isolated. Fig. 7 shows the instrumented test rig components. The bearingless machine along with the load motor, connected through a universal joint, are shown in Fig. 7a). At the non-drive-end of the bearingless machine, a self-alignment bearing avoids the axial and x-y

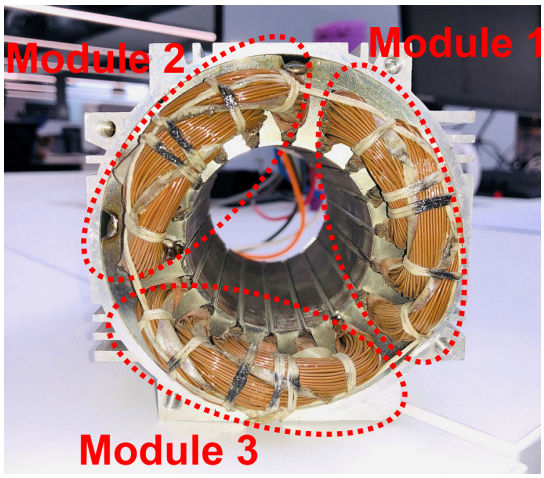

Fig. 6. The stator of the bearingless machine.

displacement of the shaft. The two degrees of the freedom radial movement of the shaft is allowed at the drive-end but it is limited by a backup bearing with a clearance of $150\mu m$. The rotor radial $x-y$ positions are measured via two 3300 XL NSv proximity transducers which are also called eddy current sensors, as shown in Fig. 7c). The main parameters of the proximity transducers are 10kHz bandwidth, a linear range from 0.25 to 1.75 mm and an Incremental Scale Factor of 7.87V/mm. A cylinder of AISI 4140 is mounted on the shaft to maximise the measurement performance, being the sensor calibrated in the factory for acting on this material. The rotor x-y axis positions are regulated by two independent conventional PID controllers [25]. A digital low pass filter is installed in the position controllers to limit the effect of the measurement noise, acquired from the proximity transducers, on the differential component of the position PID controllers.

This article has been accepted for publication in IEEE Transactions on Industrial Electronics. This is the author's version which has not been fully edited and content may change prior to final publication. Citation information: DOI 10.1109/TIE.2021.3097610

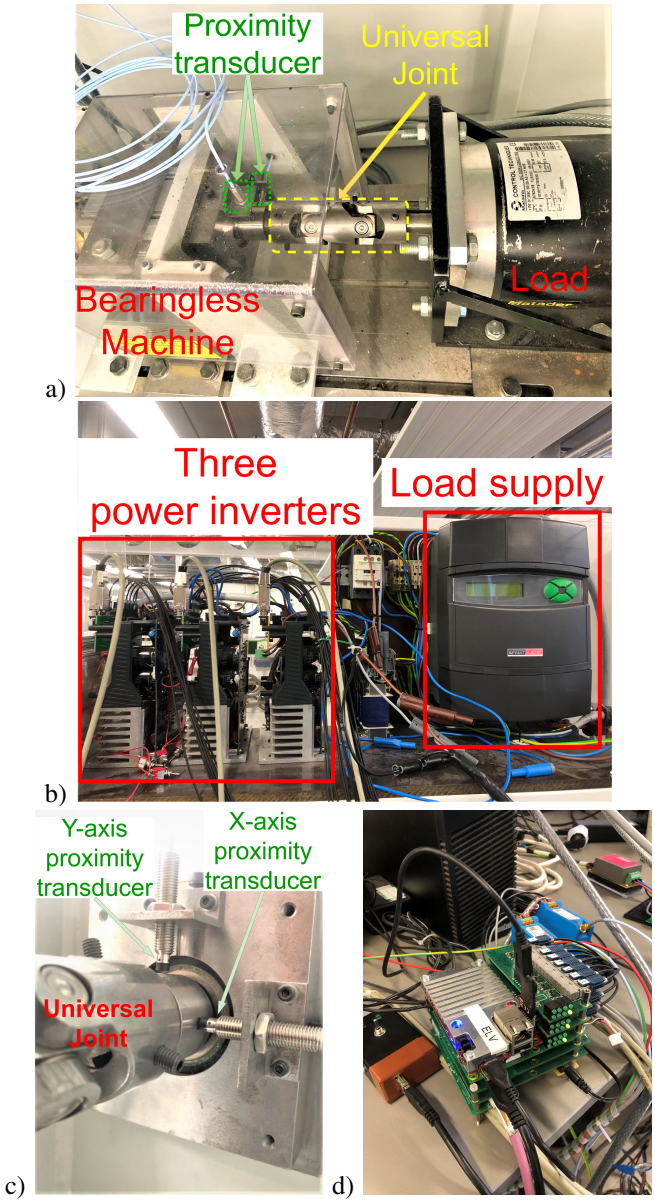

Fig. 7. a) Bearingless machine and the motor load, b) three power inverters for bearingless machine and converter for the load machine, c) proximity transducers, d) control board.

The dominant pole of the position controllers is placed in the real axis of the complex plane, 130Hz. Each sector of the bearingless machine is supplied by an independent three-phase power inverter, as shown in Fig. 7b). The inverters are SPWM modulated, and the voltage references are obtained from conventional PI current controllers. The bandwidth of the latter is 1000Hz. The custom-made control platform, where the control strategy is implemented, is based on the off-the-shelf Microzed board. This platform manages the power converters through fibre optic cables, as shown in Fig. 7d). The switching frequency is set at 10kHz.

B. Power sharing in healthy machine condition

In the first test, the speed controller is disabled and the angular shaft speed is controlled at 3000rpm by the load motor while the shaft radial position is regulated by the bearingless machine. The power sharing coefficient is kept constant during the whole experiment to $Z_{sh} = [0.5\ 0.7\ -0.2]'$. The experimental results are shown in Fig. 8. At 0.05s, the torque reference changes from 0 to $2Nm$, resulting in q-axis currents of three modules increasing from 0 to 7.8A, 10.92A and -3.12A, respectively, as shown in Fig. 8a). As explained in Sect. III, the q-axis current of each sector is determined by the power sharing coefficient and the torque reference. In the meantime, the d-axis currents increase to compensate for the radial force contribution generated by the q-axis currents, as shown in Fig. 8b). The shaft x-y axes position are displayed in Fig. 8c) showing a stable operation during the torque transient.

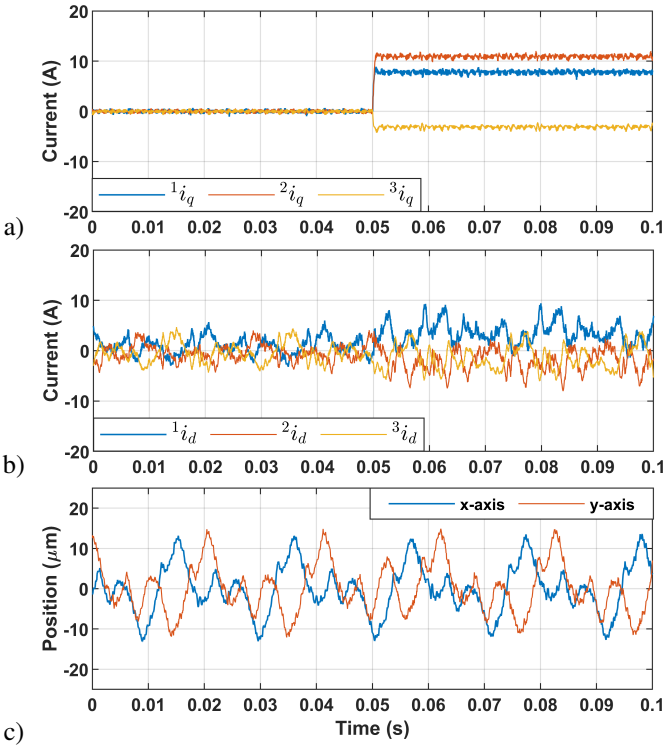

Fig. 8. Experimental results without the speed controller. a) q-axis currents of three sectors. b) d-axis currents of three sectors. c) Shaft x-y axes position.

C. Power sharing in faulty machine condition

The second test, whose results are shown in Fig. 9, verifies the performance of the power-sharing technique when an entire stator module is in open fault. The experimental results are recorded during the transient of the fault, and the pre- and post-fault operation is also included. The speed is still set at 3000rpm by the load motor while the shaft x-y position is controlled by the bearingless machine. This test is constituted by four steps as clearly shown in Fig. 9a).

- Before 0.2s, the power-sharing is set to be uniform, with 5.2A q-axis currents in all the three sectors.
- Then, the q-axis currents of three sectors separately change to -6.24A, 9.36A, and 12.48A at 0.2s due to a request of power sharing coefficients $Z_{sh} = [-0.4\ 0.6\ 0.8]'$.
- At 0.4s, the three-phase open circuit fault occurs in sub-winding 1, dropping to zero the d-q axes currents of the first module, as shown in Fig. 9a) and b), while the power sharing coefficients update to $Z_{sh} = [0\ 0.2\ 0.8]'$ resulting in

This article has been accepted for publication in IEEE Transactions on Industrial Electronics. This is the author's version which has not been fully edited and content may change prior to final publication. Citation information: DOI 10.1109/TIE.2021.3097610

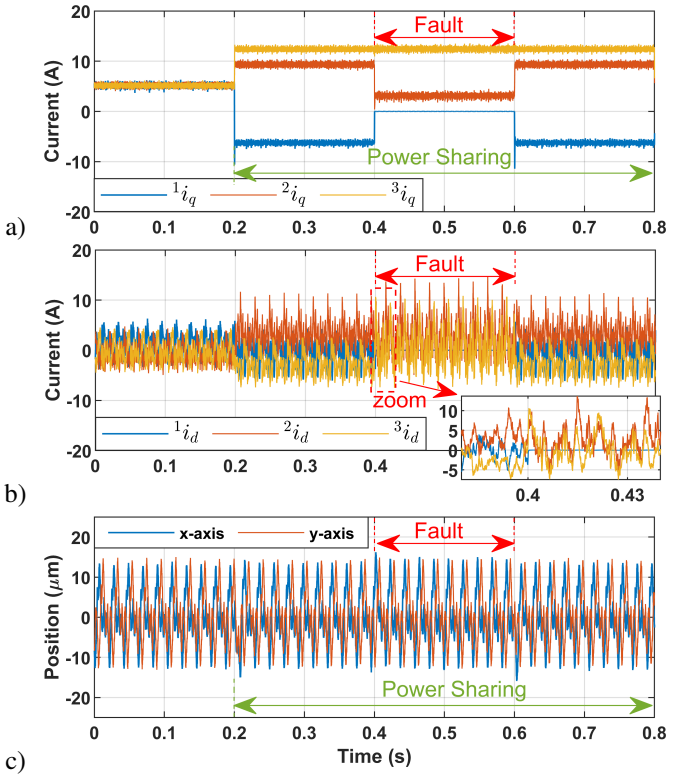

Fig. 9. Experimental results of the test without the speed controller under the three-phase open circuit fault condition. a) q-axis currents of three sectors. b) d-axis currents of three sectors. c) Shaft x-y axes position.

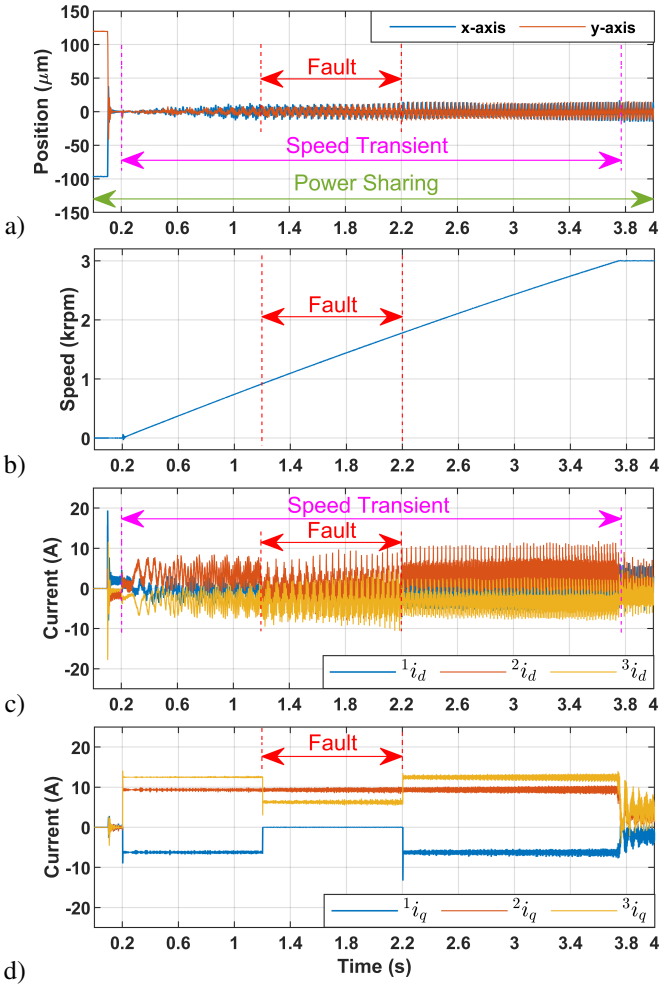

Fig. 10. Experimental results of the test with the speed controller. a) Shaft x-y axes position. b) Rotating speed. c) d-axis currents of three sectors. d) q-axis currents of three sectors.

the decrease of the i_q current of the sub winding 2 while the i_q current of inverter 3 is kept constant.

- After 0.6s, the faulty sector recovers and goes back to its normal operation. Consequently, the $d-q$ axes currents increase to the same magnitude that they had between 0.2s and 0.4s.

Three small position oscillations can be appreciated from Fig. 9 c) at 0.2s, 0.4s and 0.6s, respectively. These oscillations are caused by the sudden change in the power sharing coefficients and the open fault occurrence. However, the results clearly show that these fast current transients do not practically affect the performance of the bearingless operation.

D. Power sharing speed and position transient

During the third test, both speed and radial positions are controlled by the bearingless drive in order to asses the system behaviour in both position and speed transient under simultaneous power sharing and open module fault conditions. In particular, this test can be divided in five periods described in the following with reference to Fig. 10a-d) showing positions, speed, and $d-q$ axis currents, respectively.

- Before 0.1s, the drive is off.
- Then, at 0.1s, the drive is activated with the power sharing coefficients equal to $Z_{sh} = [-0.4\ 0.6\ 0.8]'$. The shaft moves from its rest position to the airgap centre, as shown in Fig. 10a). The radial suspension force for levitating the rotor is totally generated by the d-axis currents being null the speed set point. Thus, three peaks occur in the d-axis currents at 0.1s, as shown in Fig. 10c).
- After the position transient, the machine accelerates from 0rpm to 3000rpm between 0.2s and 3.8s. During the speed transient the machine's output torque is $2Nm$. Correspondingly, the q-axis currents of the three sectors are -6.24A, 9.36A and 12.48A, respectively, and are defined by the torque reference and sharing coefficients.
- During the speed transient at 1.2s, an open fault occurs in the first stator module, and the power sharing coefficients are changed to $Z_{sh} = [0\ 0.6\ 0.4]'$ being null the contribution of the first sub-winding.
- At 2.2s, the first module recovers from its faulty condition, and the power sharing coefficients returns back to the previous healthy value, and consequentially also the currents.
- At 3.8s, the speed transient ends, and the q axis currents decrease following the torque reduction.

The results highlight the robustness of the proposed control strategy for the power sharing operation of the bearingless drive also when a fault happens in an entire stator module during a speed transient.

VI. Conclusion

This work introduce a modular power sharing control technique for bearingless multi-three phase permanent magnet synchronous machines and demonstrates its performance also under one module open phase fault. First a comprehensive description of the radial force and torque generation principle is given, aided by a detailed FEA of the considered machine. This analysis is aimed at assessing one of the hypothesis of the control technique, i.e. the linearity of the force-current relationship. Then, the theoretical fundamentals of the proposed control strategy, allowing both bearingless and power sharing operations in healthy and faulty conditions, have been outlined. Further FEAs replicating the real control scenario have also been carried out with the aim of assessing the effect of increasing the force harmonic content used within the control in terms of quality of the force production and computational burden. The analysis also demonstrates the validity of the control hypothesis of negligible coupling between stator modules in the generation of the overall wrench. The proposed control strategy has been finally experimentally validated for a wide range of operating scenarios including the bearingless and power sharing operation, in both healthy and faulty conditions also during speed transient. These outcomes represent a step forward with respect to the methods presented in literature and introduce novel elements to be applied in fault tolerant drives for bearingless machines.

References

[1] F. Barrero and M. J. Duran, "Recent advances in the design, modeling, and control of multiphase machines—part i," *IEEE Transactions on Industrial Electronics*, vol. 63, no. 1, pp. 449–458, 2016.

[2] G. Sulligoi, A. Tessarolo, V. Benucci, A. Millerani Trapani, M. Baret, and F. Luise, "Shipboard power generation: Design and development of a medium-voltage dc generation system," *IEEE Industry Applications Magazine*, vol. 19, no. 4, pp. 47–55, 2013.

[3] E. Levi, "Multiphase electric machines for variable-speed applications," *IEEE Transactions on Industrial Electronics*, vol. 55, no. 5, pp. 1893–1909, 2008.

[4] A. Salem and M. Narimani, "A review on multiphase drives for automotive traction applications," *IEEE Transactions on Transportation Electrification*, vol. 5, no. 4, pp. 1329–1348, 2019.

[5] A. Tessarolo, L. Branz, and M. Bortolozzi, "Stator inductance matrix diagonalization algorithms for different multi-phase winding schemes of round-rotor electric machines part i. theory," in *IEEE EUROCON 2015 - International Conference on Computer as a Tool (EUROCON)*, 2015, pp. 1–6.

[6] J. W. Bennett, G. J. Atkinson, B. C. Mecrow, and D. J. Atkinson, "Fault-tolerant design considerations and control strategies for aerospace drives," *IEEE Transactions on Industrial Electronics*, vol. 59, no. 5, pp. 2049–2058, 2012.

[7] M. J. Duran, I. González-Prieto, A. González-Prieto, and F. Barrero, "Multiphase energy conversion systems connected to microgrids with unequal power-sharing capability," *IEEE Transactions on Energy Conversion*, vol. 32, no. 4, pp. 1386–1395, 2017.

[8] I. Zoric, M. Jones, and E. Levi, "Arbitrary power sharing among three-phase winding sets of multiphase machines," *IEEE Transactions on Industrial Electronics*, vol. 65, no. 2, pp. 1128–1139, 2018.

[9] G. Sala, M. Mengoni, G. Rizzoli, L. Zarri, and A. Tani, "Decoupled d–q axes current-sharing control of multi-three-phase induction machines," *IEEE Transactions on Industrial Electronics*, vol. 67, no. 9, pp. 7124–7134, 2020.

[10] B. Wang, J. Wang, A. Griffo, and B. Sen, "A general modeling technique for a triple redundant 3×3-phase pma synrm," *IEEE Transactions on Industrial Electronics*, vol. 65, no. 11, pp. 9068–9078, 2018.

[11] Y. Shi, J. Wang, R. Hu, and B. Wang, "Electromagnetic and thermal behavior of a triple redundant 9-phase pmasynrm with insulation deterioration fault," *IEEE Transactions on Industry Applications*, vol. 56, no. 6, pp. 6374–6383, 2020.

[12] H. Zhang, P. Giangrande, G. Sala, Z. Xu, W. Hua, V. Madonna, D. Gerada, and C. Gerada, "Thermal model approach to multisector three-phase electrical machines," *IEEE Transactions on Industrial Electronics*, vol. 68, no. 4, pp. 2919–2930, 2021.

[13] S. Kobayashi, M. Ooshima, and M. N. Uddin, "A radial position control method of bearingless motor based on d - q -axis current control," *IEEE Transactions on Industry Applications*, vol. 49, no. 4, pp. 1827–1835, 2013.

[14] M. Ooshima, A. Kobayashi, and T. Narita, "Stabilized suspension control strategy at failure of a motor section in a d-q axis current control bearingless motor," in *2015 IEEE Industry Applications Society Annual Meeting*, 2015, pp. 1–7.

[15] H. Mahmoud, G. Valente, M. Degano, M. D. Nardo, C. Gerada, and B. James, "Multi-sector windings for bearing relief e-machine: Saturation and cross coupling effects," in *2020 International Conference on Electrical Machines (ICEM)*, vol. 1, 2020, pp. 246–252.

[16] H. Mitterhofer, W. Gruber, and W. Amrhein, "On the high speed capacity of bearingless drives," *IEEE Transactions on Industrial Electronics*, vol. 61, no. 6, pp. 3119–3126, 2014.

[17] N. Kurita, T. Ishikawa, N. Saito, T. Masuzawa, and D. L. Timms, "A double-sided stator type axial bearingless motor development for total artificial heart," *IEEE Transactions on Industry Applications*, vol. 55, no. 2, pp. 1516–1523, 2019.

[18] A. Chiba, T. Fukao, O. Ichikawa, M. Oshima, M. Takemoto, and D. Dorrell, *Magnetic Bearings and Bearingless Drives*. Elsevier Science, 2005.

[19] W. K. S. Khoo, K. Kalita, and S. D. Garvey, "Practical implementation of the bridge configured winding for producing controllable transverse forces in electrical machines," *IEEE Transactions on Magnetics*, vol. 47, no. 6, pp. 1712–1718, 2011.

[20] E. L. Severson, R. Nilssen, T. Undeland, and N. Mohan, "Design of dual purpose no-voltage combined windings for bearingless motors," *IEEE Transactions on Industry Applications*, vol. 53, no. 5, pp. 4368–4379, 2017.

[21] J. Huang, B. Li, H. Jiang, and M. Kang, "Analysis and control of multiphase permanent-magnet bearingless motor with a single set of half-coiled winding," *IEEE Transactions on Industrial Electronics*, vol. 61, no. 7, pp. 3137–3145, July 2014.

[22] E. Severson, S. Gandikota, and N. Mohan, "Practical implementation of dual-purpose no-voltage drives for bearingless motors," *IEEE Transactions on Industry Applications*.

[23] G. Sala, G. Valente, M. Di Nardo, M. Degano, P. Zanchetta, and C. Gerada, "Power-sharing control in bearingless multi-sector and multi-three-phase permanent magnet machines," *IEEE Transactions on Industrial Electronics*, pp. 1–1, 2020.

[24] S. Serri, A. Tani, and G. Serra, "Analytical model of radial forces considering mutual effects between torque and levitation current space vectors in 5-phase pm bearingless motors," in *IECON 2013 - 39th Annual Conference of the IEEE Industrial Electronics Society*, Nov 2013, pp. 5142–5147.

[25] G. Valente, A. Formentini, L. Papini, P. Zanchetta, and C. Gerada, "Position control study of a bearingless multi-sector permanent magnet machine," in *IECON 2017 - 43rd Annual Conference of the IEEE Industrial Electronics Society*, 2017, pp. 8808–8813.

Zhuang Wen (Student Member, IEEE) received the Bachelor's degree in Electrical Engineering and its Automatization from Taiyuan University of Science and Technology, China, in 2012, Master's degree in Electrical Engineering from the University of Nottingham, U.K., in 2014. He is currently working toward his Ph.D. degree with the Power Electronics, Machines and Control Group, University of Nottingham, U.K. His main research interest is the control of bearingless electrical machines.

This article has been accepted for publication in IEEE Transactions on Industrial Electronics. This is the author's version which has not been fully edited and content may change prior to final publication. Citation information: DOI 10.1109/TIE.2021.3097610

Mauro Di Nardo (Member, IEEE) received the M.Sc. (Hons.) degree in electrical engineering from the Polytechnic University of Bari, Italy, in 2012, and the Ph.D. degree in electrical machine design from the University of Nottingham, U.K., in 2017. From 2017 to 2019, he was Head with the AROL R&D Team within the Polytechnic University of Bari leading industrial projects on electrical drives design for mechatronics applications. Since the 2019, he is with the Power Electronics and Machine Control Group of the University of Nottingham as Research Fellow working on wide variety of projects of high industrial and scientific impacts. His research interests include the analysis, modelling, and design optimizations of permanent magnet and synchronous reluctance machines for automotive, aerospace and household sectors, induction motor for industrial applications as well as niche machine topologies such as bearingless and hysteresis motor.

Giacomo Sala (Member, IEEE) received the Ph. D. in Electrical Machines and Drives in 2018 from the University of Bologna, Italy. He worked as a researcher until 2019 in the Power Electronics, Machines and Control Group, Department of Electrical and Electronic Engineering, The University of Nottingham. Since 2019 he has been working as a researcher with the Department of Electrical, Electronic, and Information Engineering "Guglielmo Marconi" - DEI, University of Bologna, Italy, where he is currently employed as a Junior Assistant Professor, since 2020. His research interests include design, modelling and control of multiphase electrical machines, fault tolerant controls and fault diagnosis of electric drives.

Giorgio Valente received the Master degree (Hons.) in electrical engineering from the University of Padova, Padova, Italy, in 2014, and the Ph.D. degree in electrical machines design and control from the University of Nottingham, Nottingham, U.K., in 2018. He then worked for two years as a Research Fellow with the Power Electronics, Machines and Control Group, University of Nottingham. He is currently an Electric Machine Design and Development Engineer with Romax Technology Ltd, Nottingham, U.K. His research interests include bearingless machines design and control, high speed machines, traction machines, and multiphysics-based optimization of electrical machines

Alessandro Marfoli received the M.Sc. in Electrical Engineering from the University of Pisa, Italy, in 2015 and the Ph.D. degree in electrical machine design from the University of Nottingham (UK) in 2020. He is currently a Research Fellow within the same institution working on wide variety of projects of high industrial and scientific impacts. His main research interests involves the modelling, analysis and optimization of electrical machines including induction and synchronous machines also for bearingless applications.

Michele Degano SM'12) received his Master's degree in Electrical Engineering from the University of Trieste, Italy, in 2011, and his Ph.D. degree in Industrial Engineering from the University of Padova, Italy, in 2015. Between 2014 and 2016, he was a postdoctoral researcher at The University of Nottingham, UK, where he joined the Power Electronics, Machines and Control (PEMC) Research Group. In 2016 he was appointed Assistant Professor in Advanced Electrical Machines, at The University of Nottingham, UK. He was promoted Associate Professor in 2020. His main research focuses on electrical machines and drives for industrial, automotive, railway and aerospace applications, ranging from small to large power. He is currently the PEMC Director of Industrial Liaison leading research projects for the development of hybrid electric aerospace platforms and electric transports.

Pericle Zanchetta (Fellow, IEEE) received the M.Eng. degree in electronic engineering and the Ph.D. degree in electrical engineering from the Technical University of Bari, Bari, Italy, in 1993 and 1997, respectively. In 1998, he was an Assistant Professor of Power Electronics with the Technical University of Bari. In 2001, he was a Lecturer in Control of Power Electronics Systems with the PEMC Research Group, The University of Nottingham, where he is currently a Professor in Control of Power Electronics Systems. He is also a Part Time Professor with the University of Pavia, Pavia, Italy. He has authored or coauthored more than 350 peer reviewed papers, he is the Past Chair of the IEEE-IAS Industrial Power Converter Committee IPCC (2016–2017), the Transactions Review Chair for IPCC (2018–2021). He is also the Chair of the IEEE-IAS Industrial Power Conversion Systems Department IPCSD 2020-2021. His research interests include control and optimization of power converters and drives, matrix and multilevel converters. He is IEEE Fellow Class 2019.

Chris Gerada SM'12) is an Associate Pro-Vice-Chancellor for Industrial Strategy and Impact and Professor of Electrical Machines. His principal research interest lies in electromagnetic energy conversion in electrical machines and drives, focusing mainly on transport electrification. He has secured over £20M of funding through major industrial, European and UK grants and authored more than 350 referred publications. He received the Ph.D. degree in numerical modelling of electrical machines from The University of Nottingham, Nottingham, U.K., in 2005. He subsequently worked as a Researcher with The University of Nottingham on high-performance electrical drives and on the design and modelling of electromagnetic actuators for aerospace applications. In 2008, he was appointed as a Lecturer in electrical machines; in 2011, as an Associate Professor; and in 2013, as a Professor at The University of Nottingham. He was awarded a Research Chair from the Royal Academy of Engineering in 2013. Prof. Gerada served as an Associate Editor for the IEEE TRANSACTIONS ON INDUSTRY APPLICATIONS and is the past Chair of the IEEE IES Electrical Machines Committee.